Chemical Engineering Journal 391 (2020) 123478

Contents lists available at ScienceDirect

Chemical Engineering Journal

journal homepage: www.elsevier.com/locate/cej

Multi-stimuli-responsive liquid marbles stabilized by superhydrophobic luminescent carbon dots for miniature reactors

Zhijian Zhao[a,b], Shaowei Qin[a,b], Dan Wang[a,b,*], Yuan Pu[a,b], Jie-Xin Wang[a,b], Joshua Saczek[c], Adam Harvey[c], Chen Ling[d], Steven Wang[d,*], Jian-Feng Chen[a,b]

[a] Beijing Advanced Innovation Center for Soft Matter Science and Engineering, State Key Laboratory of Organic Inorganic Composites, Beijing University of Chemical Technology, Beijing 100029, China
[b] Research Center of the Ministry of Education for High Gravity Engineering and Technology, Beijing University of Chemical Technology, Beijing 100029, China
[c] School of Engineering, Newcastle University, Newcastle upon Tyne, UK
[d] Department of Mechanical Engineering, City University of Hong Kong, Hong Kong, China

HIGHLIGHTS

- A new class of liquid marbles using luminescent carbon dots are made for chemical reactions.
- Remote control of liquid marbles using external stimuli is realized.
- Liquid marbles exhibit excellent photothermics, fluorescence and diamagnetism.
- Collisions of liquid marbles triggered by external stimuli intensify chemical reactions massively.
- Ultra high selectivity and fast reaction can be realized simultaneously by using our liquid marbles.

ARTICLE INFO

Keywords:
Liquid marbles
Luminescent carbon dots
Miniature reactor
Multi-stimuli-responsive

ABSTRACT

Remote control of microfluidic locomotion by external stimuli is attracting extensive attention due to its practical applications in various areas such as chemical reactors, gas sensors and transporters. Within this report we describe an effective method of preparing liquid marbles (LMs) stabilized by super-hydrophobic luminescent carbon dots (CDs) and demonstrate their outstanding photothermics, fluorescence and diamagnetism. The super-hydrophobic CDs were synthesized by surface functionalization using polyhedral oligomeric silsesquioxane (POSS) and manipulation of the LMs was achieved using light, electricity and magnetism. LMs could act as ideal models of collision-triggered miniature reactors for enhanced chemical reactions, with fast mixing of microfluidics leading to substantial improvement in reaction rate and selectivity. For the first time, the use of collisions triggered by multi-external stimuli has been demonstrated, showing an intensification to the micromixing process and therefore an enhancement to the microreactions. We expect that these LMs can be applicable in microfluidics, miniaturized reactors and many other associated industries.

1. Introduction

Liquid marbles (LMs) were first reported by Aussilous and Quéré in 2001, showing microfluidic motion without wetting solid surfaces. LMs have attracted increasing research interest ever since, this is due to their advantages: preventing contact with supporting surfaces, reducing surface contamination, decreasing reaction volume and time [40] and significantly reducing surface friction [1–4]. LMs are responsive to external stimuli such as gravity [5], electricity [6,7], light [8], ultrasonic waves and magnetism based on the liquid or component attributes [9,10]. However, most LMs reported only respond to a single external stimulus [11–13]. Not only can multi-responsive LMs widen the controllable range and improve the degree of precision [12], but it also provides ways of assembling multi-responsive microfluid into larger dynamic reactors [36]. The formation of LMs triggered by multiple stimuli is desirable for their application in fields such as microfluidic transportation [14], miniature reactors [15], and sensors [16]. LMs acting as “droplet reactors” have been developed recently due to

* Corresponding authors at: Beijing Advanced Innovation Center for Soft Matter Science and Engineering, State Key Laboratory of Organic Inorganic Composites, Beijing University of Chemical Technology, Beijing 100029, China (D. Wang).
E-mail addresses: wangdan@mail.buct.edu.cn (D. Wang), steven.wang@cityu.edu.hk (S. Wang).

https://doi.org/10.1016/j.cej.2019.123478
Received 2 August 2019; Received in revised form 25 October 2019; Accepted 11 November 2019
Available online 13 November 2019
1385-8947/

their advantages of compartmentalization, miniaturization, mono-dispersity and high throughput [17,18]. This helps reduce the use of chemical reagents, shows no amplification effect and allow for precise control of reaction condition [19–22]. Extensive efforts have been made recently to develop the applications/functions of LMs such as fabricating catalytic LMs to improve catalytic efficiency [19], enhancing mass transportation via dynamic rotating LMs and controlling temperature precisely in photothermal miniature reactors [23–25]. However, existing research is mainly based on either static properties of LMs or LMs-based microreactions in an individual reaction system; which limits LMs' performance as microreactors because mass transfer and molecular mixing are crucial in chemical engineering process [25]. When multiple LMs are considered the interactions between them vary greatly and depend on the properties of the coating particles as well as the liquid encapsulated within.

Coalescence between LMs is one of the most essential manipulation schemes to functionalize microfluidics, especially for use in micromixing and microreaction [26]. When two LMs are placed in contact, they will not coalesce naturally even when pressed against each other. However, surface deformation caused by collision will transfer kinetic energy to the internal reagents, triggering and even intensifying the reaction processes [27]. Numerous techniques for colliding LMs have been reported, using magnetic forces and DC voltage [28,29]; whereas the use of dynamic coalescence to intensify microreactions in LMs is rarely reported.

Herein, it is reported that a new set of LMs stabilized by super-hydrophobic luminescent carbon dots (CDs) exhibit excellent photothermic, fluorescence and diamagnetism. The CDs were functionalized with polyhedral oligomeric silsesquioxane (POSS) to serve as the super-hydrophobic shell of the LMs. The technique used within this report combined the properties of CDs with the hydrophobic properties of POSS to manipulate microfluidics in the form of LMs. Since CDs@POSS nanoparticles could be multi-stimuli-responsive to light, electricity and magnetism; CDs@POSS LM-based microreactors could be manipulated in different ways meaning that more precise control could be achieved. In this study, the collision effects on reaction rate, reaction selectivity and size of products was investigated by both simulation and experimental studies. Moreover, the luminescent property of CDs allows the LMs to act as photocatalytic microreactors, which in turn, allowed for the demonstration of photodegradation of methylene blue inside the LMs. This work opens the way for expansion on the functions of LMs and offers analysis tools to study the mechanisms of micromixing in a large variety of applications.

2. Materials and methods

2.1. Materials

Citric acid (CA), ethylenediamine (EDA), hydrazine hydrate (HHA), ethanol (EAL), tetrahydrofuran (THF), trichloromethane (TCM) and N,N′-Dicyclohexylcarbodiimide (DCC) were purchased from Sigma-Aldrich. Maleamic acid-isobutyl polyhedral oligomeric silsesquioxane (POSS) was purchased from Hybrid Plastics, Inc. (Hattiesburg, MS, USA). All the chemicals were used as received without further purification. Deionized water prepared by a Hitech Laboratory Water Purification System DW100 (Shanhai Hitech Instruments Co. Ltd), was used for all experiments.

2.2. Synthesis of luminescent CDs

Luminescent CDs were prepared from citric acid and ethylenediamine as reactants in a stirred-tank reactor (STR). Following this, 6 g of CA were dissolved in 9 mL of water within a 50 mL STR. Next, 9 mL of EDA were added at room temperature. The mixture was then heated to boil for 30 min and the reaction products were then cooled down to room temperature; obtaining the dark brown CD solids.

2.3. Synthesis of CDs@POSS

The aqueous solution of N-CD (200 mL, 2.5 mg/mL) was added to the 250 mL round-bottom flask. Next, 15 mL of HHA were added at room temperature. After being vigorously stirred for a few minutes, the mixed solution underwent a heated reflux reduction reaction at 80 °C for 6 h. Then, excessive HHA was removed by dialysis; the reduced CD (R-CDs) powders were obtained by vacuum drying. Next, the POSS structures were covalently grafted to R-CDs via the dehydration reaction between the oxygen-containing groups of POSS and surface functional groups of the R-CDs with the formation of amides and esters by using DCC as the catalyst. Typically, 1 g of POSS powder was dissolved in 100 mL THF in a 250 mL round-bottom flask. Following this, 10 mL of aqueous R-CDs solution (10 mg/mL) and 100 mg DCC were added, followed by ultrasonication treatment for 15 min. The mixture was then refluxed at 65 °C for 72 h. The solids from the mixture were then obtained by rotating evaporation, and then washed with ethanol followed by collecting the supernatant by centrifugation at 10000 rpm for 5 min. The steps were repeated three times to remove the POSS and DCC residues. Deionized water was then added to the EAL mixture solution and the superhydrophobic POSS-grafted CDs nanocomposites (CDs@POSS) were collected by centrifugation at 10000 rpm for 5 min. The precipitates were then washed by water at least twice to remove the unmodified CDs and dried in a vacuum oven (50 °C) for 12 h to obtain the final products for further use.

2.4. Characterization

The transmission electron microscope (TEM) images were taken using a Hitachi HT-7700 TEM operating in bright field mode with an accelerating voltage of 120 kV. X-ray diffraction (XRD) analysis was performed on a Shimadzu XRD-6000 diffractometer. Fourier-transform infrared (FTIR) spectra were measured by a Bruker Vector-70v FTIR spectrometer. X-ray photoelectron spectroscopy (XPS) measurements were performed on a VG Microtech ESCA 2000 instrument using a monochromic Al X-ray source. Thermogravimetric analyses (TGA) of samples were carried out using a VET ZSCh-SAT 449c instrument; at a heating rate of 10 °C·min nitrogen. The magnetic properties of the samples were investigated using a vibrating sample magnetometer (Physical Property Measurement System DynaCool, Quantum Design). A Shimadzu UV-2600 UV–Vis spectrometry was used to measure the UV–Vis transmittance spectra.

2.5. Preparation of CDs@POSS-based LMs

The LMs were fabricated by rolling the droplet on the slope or vibrating surface spread with super-hydrophobic particles. With droplets continuously rolling on the surface, abundant LMs could be made for practical applications.

2.6. CFD simulation procedure

All simulations were carried out by a commercial software, Fluent 18.2. The SIMPLE algorithm was applied to solve pressure-velocity coupling equations, whereas, PRESTO was employed for discretization of pressure Poisson equation while first order upwind was used for discretization of the rest of equations. Each simulation was conducted for 2000-time steps with a time step size of 2×10^{-5} s. A total of 30 max iterations were performed per step to guarantee calculation convergence. A grid of 91,278 cells was obtained after grid independence validation and the final 2D computational grids generated were all tetrahedron unstructured grids. Computing domains were all set as stable walls. The convergence criterion of the simulation was assumed when the values of all governing equations' residuals were less than 10^{-3}.

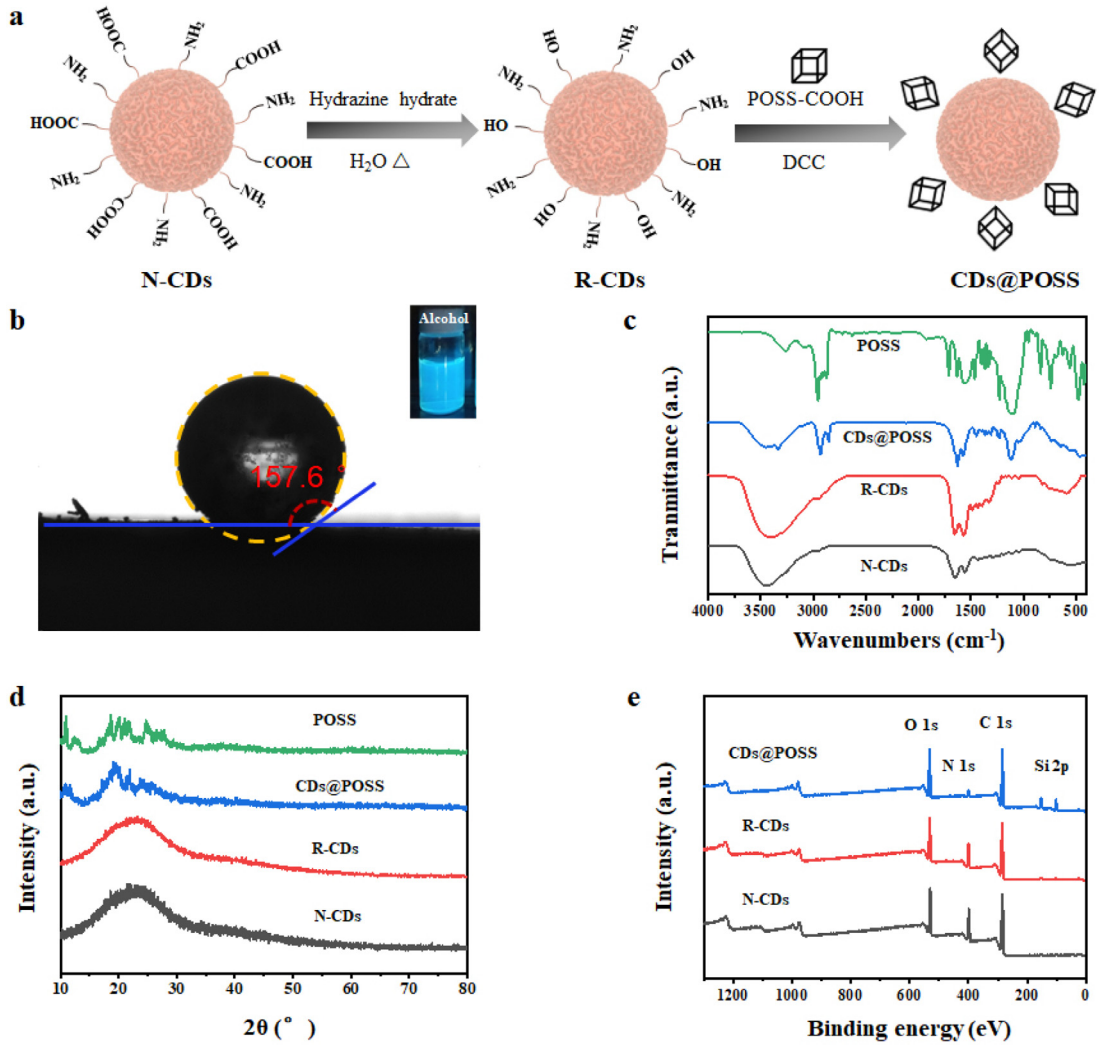

Fig. 1. (a) Synthesis process of CDs@POSS. (b) Water droplet on CDs@POSS powders and air/water contact angle. The inset shows the fluorescence of CDs@POSS in organic solvent. (c) FTIR, (d) XRD and (e) XPS spectra of N-CDs, POSS, R-CDs and CDs@POSS.

3. Results and discussion

3.1. Characterization

Hydrophobic particles based on CDs were developed. Luminescent CDs were synthesized by accepted methods using CA and EDA as the starting materials [30]. The superhydrophobic CDs@POSS nanocomposites were synthesized via a two-step synthetic approach shown in Fig. 1a. The carboxyl groups on the surface of the CDs were reduced and the presence of surface amidogen and hydroxyl on the CDs allowed for the grafting of carboxyl-functionalized POSS. This allowed for the formation of hydrophobic CDs-POSS nanocomposites via condensation and esterification reactions. The static contact angles of water drop on the CDs@POSS powders were measured to be 157.6° (Fig. 1b), indicating the super-hydrophobic property of this materials.

The FTIR spectra in Fig. 1c reveals the characteristic peaks of –COOH (1652 cm^{-1} and 3438 cm^{-1}) and –NH (1550 cm^{-1}) in N-CDs and R-CDs. They also show decreasing –COOH in R-CDs by the reduction of HHA. POSS and CDs@POSS had very similar characteristic peaks, demonstrating that POSS has been successfully grafted on the surface of CDs. This conclusion is also confirmed in Fig. 1d, which reproduced the XRD patterns for CDs, POSS and N-CDs/POSS. The broad peak was characteristic of CDs of a quantum size. XPS measurements were used to verify the chemical composition and surface electronic state. The survey scan spectrum verified the existence of C, N, Si, O in the composite with atom percentages of 61.8%, 4.2%, 14.2% and 11.8%, respectively (Fig. 1e). More details can be seen in Table S1.

TEM was then used to characterize the morphologies of the prepared samples. Fig. 2a shows dot-like morphology with an average size of 2.5 nm. After grafting with POSS, the composite showed a size of 6.6 nm with agglomeration (Fig. 2b). Thermogravimetric analysis indicated the calculated weight ratio of CDs and POSS in the nanocomposites as 2:3 (Fig. 2c), showing that one carbon dot may become grafted with several layers of POSS. The differences in fluorescence between samples (N-CDs, R-CDs and CDs@POSS) are shown in Fig. 3, all indicated an emission wavelength of 455 nm. After grafting, the excitation wavelength at 255 nm was no longer present and redshift at 365 nm was measured; while the absolute quantum efficiency remained at 25.46% (Table S2). The fluorescence stability was enhanced after grafting due to the POSS layer protecting carbon dots from ultraviolet damage (Fig. S1).

3.2. Multi-stimuli responsiveness of CDs@POSS-based LMs

Herein, the performance of multi-stimuli-responsive CDs@POSS-based LMs for the remote control of microfluidics is described in Fig. 4. To demonstrate this, LMs were prepared by coating 10 μL droplets with CDs@POSS particles and suspended on water statically. External

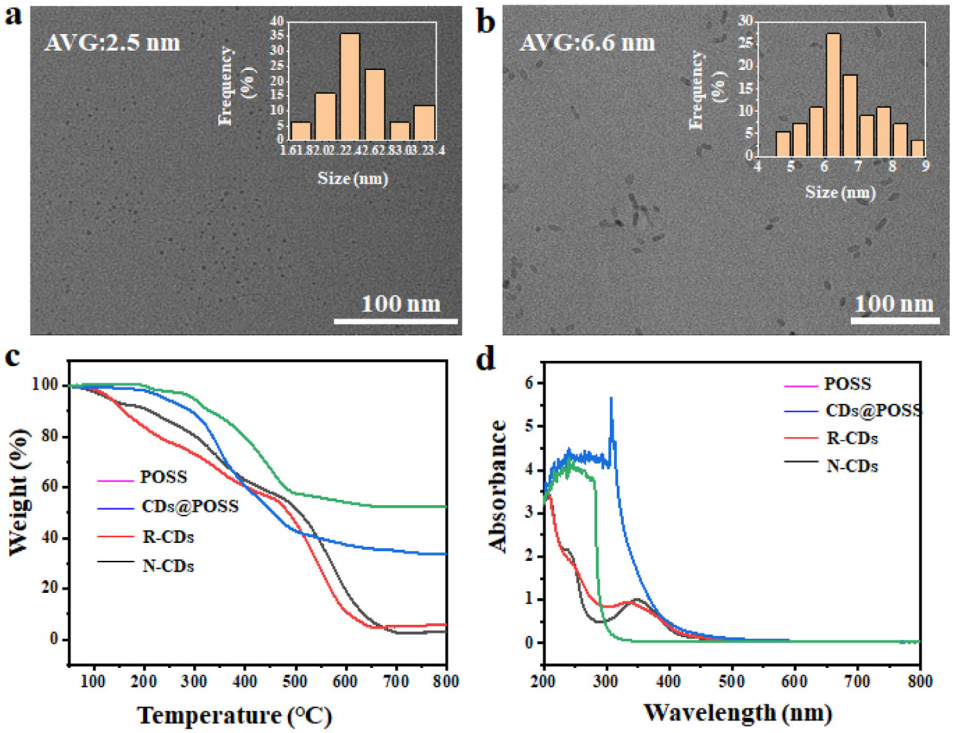

Fig. 2. TEM images of (a) N-CDs, (b) CDs@POSS, the inserts show the distribution of particles size. (c) TGA of POSS, N-CDs, R-CDs and CDs@POSS. (d) UV–Vis spectra of POSS, N-CDs, R-CDs and CDs@POSS.

stimuli including electricity, light and magnetism were then applied respectively to induce movement of the LMs (Fig. 4a and Supplementary Videos). For a more in-depth understanding of the multi-stimuli-responsive process of CDs@POSS-based LMs, the mechanism of each external stimuli was explored (Fig. 5).

3.2.1. Light-driving locomotion of LMs

For a light-driving locomotive process, the direction of LMs could be controlled simply by moving the irradiation point on the surface. The LMs prepared by CDs@POSS acted as photothermal materials, so they could be manipulated by absorbed light [31,32]. LMs were prepared by rolling 5 μL water droplets (1.7 mm diameter) on the surface of N-CDs/POSS powders followed by transferring onto the air-water interface. Upon irradiation at an angle of ≈ 45° (980 nm laser, spot diameter: 1 mm, output power: 1310 mW), movement of the LMs could be triggered by infrared light on the air–water interface through the moving of a laser beam (Supplementary Video 1). As shown in Fig. 4b, the N-CDs/POSS-coated LM was placed in a Petri-dish filled with water and irradiated by light with its motion traced. The maximum velocity of the LM was 12 $mm{\cdot}s^{-1}$ and its direction could be modulated sensitively by altering the angle of irradiation, during which process a push or pull effect could be observed. Light-responsive control with sensitivity makes it a promising application in light-induced microfluidic transport.

To explore the mechanism of light-induced locomotion process, the heat distribution upon irradiation is studied. Fig. 5b displays typical thermography snapshots of light-driving locomotion of CDs@POSS-coated LMs on the water surface. At t = 0 s, the LMs were in the thermal equilibrium with the water around them. Once irradiated by a NIR laser (t > 0 s), the temperature of N-CDs/POSS rose rapidly, simultaneously heating the water surface nearby and thus triggering heat convection to transport LMs. Fig. 5b indicates that the LMs irradiated by NIR could reach 30–35 °C and a heat trail could be identified from the motion trace. The remarkable thermal difference between LMs (30 °C) and the bulk water (17 °C) led to a surface tension difference at the air–water interface, causing Marangoni flow thus providing propulsion for the LMs (Fig. 5a). This is different from many other methods for light-induced motion of LMs, for example, by thermocapillary forces which relied on the photosensitive surfactant to generate Marangoni flows [38]. The LMs coated by photothermal materials were not only solvent-friendly but also able to carry loads with universality which could be applicable with more convenience [8].

Next, the locomotive process of LMs stimulated by light was quantified. Eq. (1) was applied to describe this light-induced motion [8]:

$$m\frac{d^2x}{dt^2} = \triangle\gamma w - \varepsilon v \tag{1}$$

where m, Δγ, w, ε, v are the mass of the LMs, the surface tension difference, the width of irradiated area, the friction coefficient and the velocity of the LMs, respectively. As shown in Fig. 4b and Supplementary Video 1, the velocity reached 12 $mm{\cdot}s^{-1}$ within 1 s, meaning the generated force on LMs was calculated to be 0.4 μN (the mass of LMs is 4.8 mg). The velocity is a function of light power, position, angle of laser and thickness of the LMs shell. Enhancement of the pushing force from these terms could then lead to use with practical applications.

3.2.2. Electricity-driving locomotion of LMs

In the electricity-responsive experiment, a glass bar was charged by rubbing against a silk cloth to provide the electric field. The LMs were on the surface of water when the charged glass bar approached, then followed the glass bar with the direction of movement being adjusted sensitively (Fig. 4c and Supplementary Video 2). The LMs were able to reach velocity as high as 6.4 $cm{\cdot}s^{-1}$. When the bar was removed, the LMs' movement stopped within 2 s. This move-stand cycle could be performed multiple times without any noticeable difference in behavior (Supplementary Video 2). Under an electric field, the LMs could not only move on the air–water interface, due to the reduced friction force [39], but also be manipulated on a solid surface. Supplementary Video 5 shows the motion of the single LM and the collision of two LMs, this demonstrates the application in dynamically merging microfluidics by remote control ways.

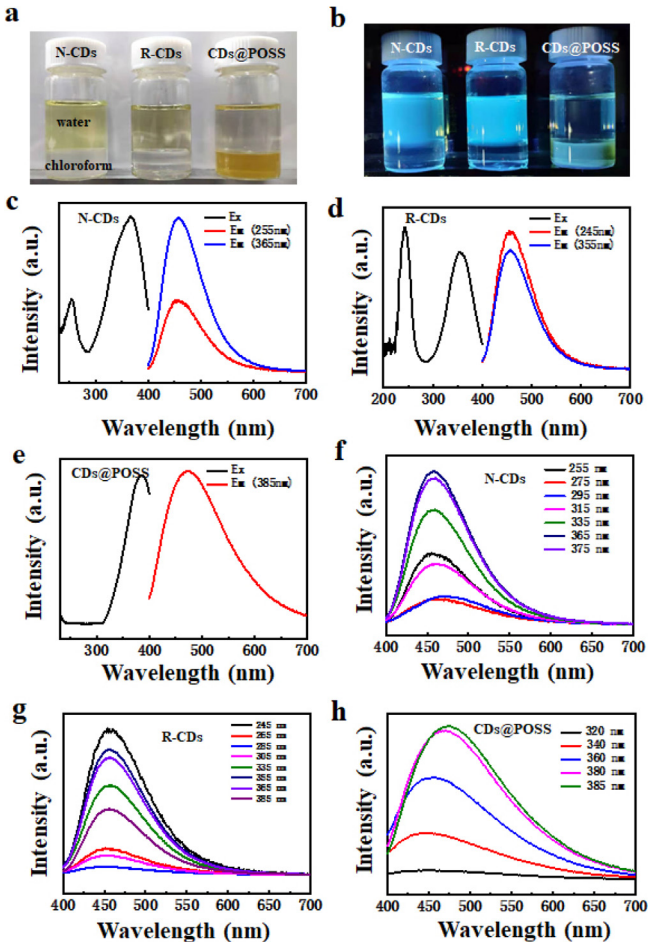

Fig. 3. (a) Solublility images of N-CD, R-CD and CD@POSS in mixture of water and chloroform and (b) their fluorescence under 365 nm irradiation. Photoluminescence excitation and emission spectrums of (c) N-CDs, (d) R-CDs and (e) CDs@POSS. Photoluminescence emission spectrums of (f) N-CDs, (g) R-CDs and (h) CDs@POSS under different excitations.

The origin of voltage-driving LMs can be explained by the electrostatic force (F_E) caused by free-charge migration (Fig. 5c). F_E was produced by the charged glass bar, which then redistributed the charge on the coated particles of the LMs; as verified via a sequence of experiments. Two LMs were placed on different sides of a Petri dish. When the LMs became closer, due to external stimulus, the two LMs agglomerate spontaneously with notable attraction (Fig. 5d and Supplementary Video 2). Fig. 5c also illustrates this agglomeration; when two LMs became close enough, the free charge redistributed due to the Coulomb force, which made heterocharge gather at the proximal edges. The electrostatic attraction then facilitated the agglomeration of the two LMs. To verify this free-charge redistribution mechanism, the charged glass bar was positioned close to the assembled LMs, leading to an equilibrium repulsion distance of 2 mm. However, removal of the glass bar caused the LMs to reassemble again (Fig. 5e). Hence, it was proved that the external field induced electrophoretic force which drived the LMs accordingly. These LMs that responded to electrical forces could be explored in a wide variety of applications.

3.2.3. Magnetism-driving locomotion of LMs

Since the carbon nanomaterials can exhibit magnetic properties such as ferromagnetism or diamagnetism [34], the CDs@POSS-coated LMs are able to respond to magnetic fields. Fig. 4d and Supplementary Video 3 illustrate experiments in which the LMs could be actuated to move in different directions slowly ($u \sim 2\ mm{\cdot}s^{-1}$). Unlike driving LMs by the superparamagnetic property of Fe_3O_4 as previously reported [33] which gives an attraction force, the LMs coated with prepared N-CDs/POSS are repelled by a magnet.

As illustrated in Fig. 5g, the magnetization was opposite to the magnetic field, which confirmed the diamagnetism of N-CDs/POSS. Pure POSS powder coated LMs were prepared to demonstrate the N-CD's role of responding to magnetism. Fig. S4 displays that the pure POSS coated LM showed no response to the magnetic field. In this work, the magnetic drive (10 μL LM, ~1000 Oe) became more evident as the magnetic field intensity got stronger. Additionally, the diamagnetic force could be used for magnetic suspension to further reduce the friction as no close contact is involved. Therefore, a flexible and sensitive transfer of microfluidic could occur based on this. It is also worth noting that, the magnetic response of LMs without metallic materials makes it more convenient and more eco-friendly to use.

3.3. Application of CDs@POSS-based LMs as microreactors

3.3.1. The role of droplets in enhancing chemical reactions

Extensive research about miniature reactors have been reported for its reduced use of chemical reagents, no amplification effect and precise control of reaction condition [21]. An explanation for these benefits was explored. Fig. 6 and Supplementary Video 6 illustrate the behavior of a droplet and water film placed on the surface of CDs@POSS powder without rolling at room temperature. When the droplet was observed, there was fine powder floating on the liquid surface acting as a tracer. This could be seen by rotation around the air-liquid interface with an observable motion ($\sim 0.5\ mm{\cdot}s^{-1}$, Fig. 6a). However, when the droplet was replaced with a thin water film, the tracer exhibited negligible fluctuation (Fig. 6b and Supplementary Video 6). The motion of the tracers were explained by computational fluid dynamics (CFD) analysis, showing that the evaporation of water would decrease the surface temperature (Fig. 6c and 6d). In the miniaturized water droplet, the thermal imbalance was more acute, thus, the surface tension difference is caused by Marangoni flow [13], which could then enhance the motion and renewal of the surface flow. The numerical simulations of both conditions revealed that fast flow exists on the external surface of the droplet and is more visible in the smaller droplet. Therefore, compared with liquid film, the liquid droplet is a better miniature reactor to accelerate the chemical reactions.

3.3.2. Microreactions in LMs intensified by collisions

As for LMs-based microreactors, coalescence is an important procedure to manipulate microfluidics in a controlled manner. This study allowed LMs to be coalesced remotely by an external stimulus to enhance miniature reactions which have rarely been reported. It is suggested that microreactions could be further intensified by collision, which was demonstrated via a facile redox reaction with significant color variation carried out as below [35]

$$S_2O_8^{2-} + 2I^- \rightarrow 2SO_4^{2-} + I_2 \quad (2)$$

$$I^- + I_2 \rightleftharpoons I_3^- \quad (3)$$

In this case, gravity-triggered collision experiments were performed for quantitative characterization (Fig. 7a). Two LMs carrying different reagents, one with potassium iodide (KI) solution and the other with potassium persulfate ($K_2S_2O_8$) solution, were placed at different vertical heights: 0 cm, 20 cm and 40 cm, respectively. The higher LM then fell to trigger the collision by gravity, with color transforming from white to yellow-brown, which confirmed the start of the chemical reaction. To further validate the execution of various conditions, UV–vis spectroscopy was carried out for 10 s after the collision. As Fig. 9a reveals, the appearance of typical absorption peaks of I^{3-} at 287 nm and 351 nm in the UV–vis absorption spectrum characterized the reaction quantitatively, with the insert snapshots recording this color variation.

More details and quantitative explorations of LM microreactors are

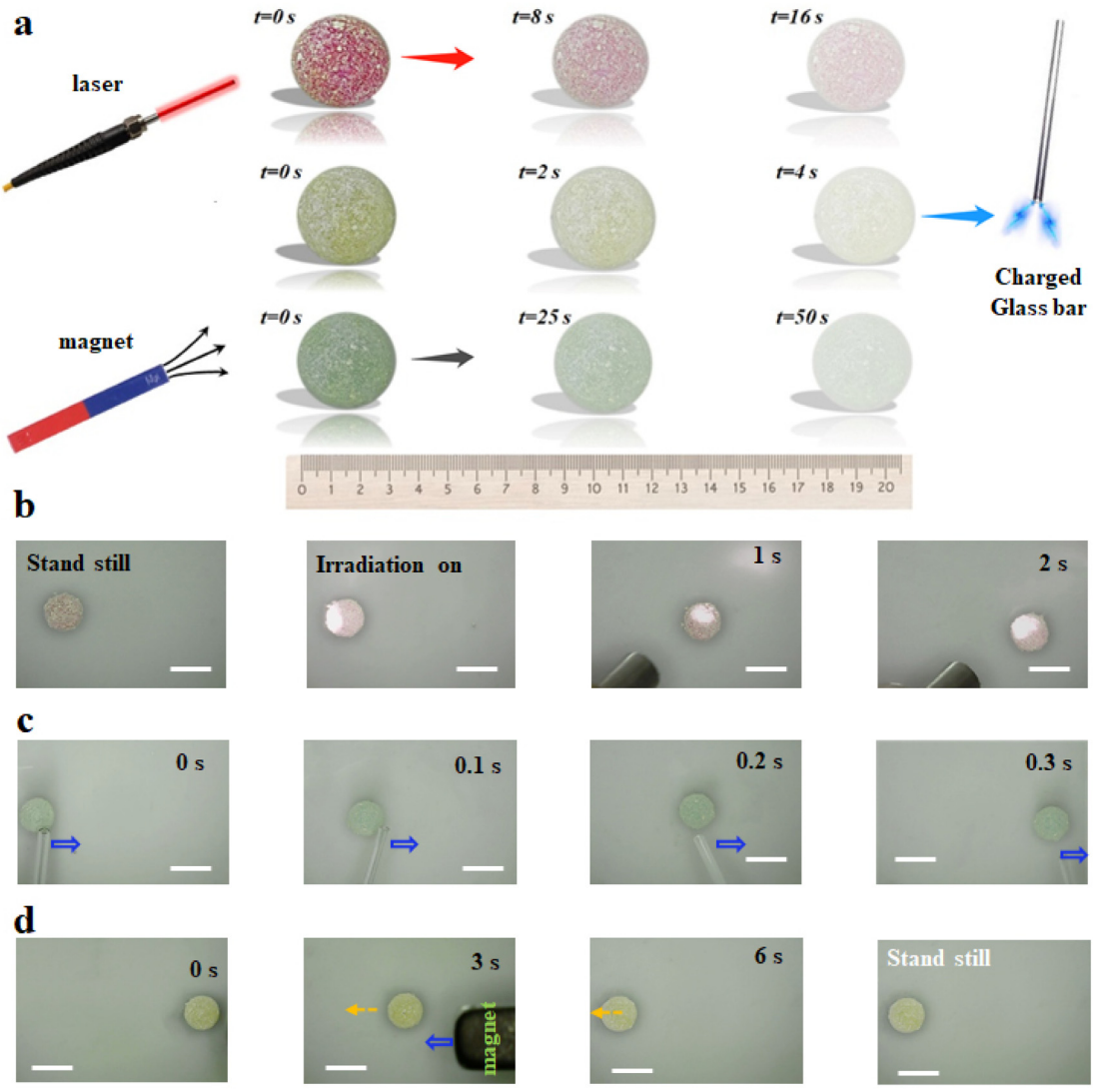

Fig. 4. (a) Scheme illustration for time-depended position of multi-stimuli-responsive LMs (charged bar, laser and magnet, respectively; the arrows represent the moving directions of LMs). Optical images of three regimes for LM manipulation: (b) light, (c) electricity, (d) magnetism; t = 0 s indicates the moment of locomotion; The solution inside LMs was dyed by methylene blue, rhodamine B and $FeCl_3$ respectively. All scale bars are 5 mm. (For interpretation of the references to color in this figure legend, the reader is referred to the web version of this article.)

shown in Fig. S2a and S2b, which exhibit the effects of vertical height and drop size respectively on reaction rates upon collisions of LMs. All experiments showed that the LM microreactor obtained a higher yield compared with bulk solution. More specifically, when the height was increased or the drop minimized, a higher yield and a more uniform product (see from the standard deviations) was obtained. Moreover, as is shown in Fig. S3, the calcium carbonate ($CaCO_3$) particles were reduced from 5.6 μm to 67 nm, this is due to the reaction moving from a stir tank reactor to 40 μL LMs, which demonstrated that the uniform distribution of reactant is also beneficial to nanoparticle preparations. Similarly, the particles became smaller as the collision height increased and drop minimized. This is because the enhanced reaction can be attributed to efficient micromixing and mass transfer process [25]. CFD simulation of two droplets' collisions triggered by gravity reflected the violent turbulent motion in LMs (Fig. 8), which was in accordance with the phenomenon observed in previous study [27]; so the enhanced inertial flow is believed to be the source of intensified mixing effect.

A novel scheme that used external stimuli besides gravity to trigger a collision between two LMs is shown in Fig. 7c, allowing for the intensified microreactions to be induced remotely in various ways. Experiments were implemented using electric stimulus, in which a higher speed was reached to achieve the coalescence of LMs (Fig. 7d). In this experiment, a LM was driven to collide and coalesce with another. The coalesced LM was shaped like a spheroid which can still be rolled and transferred by tilting the glass plate, for example. Fig. S5 and S6 also present the transformation between solid and liquid surfaces, thus extending the applications of LMs as an effective transfer tool. Based on these findings, it is believed that various stimulus like light and magnetism could have potential to trigger the coalescence of LMs. This study of the collision between liquid drops at an operational scale is believed to introduce new ways of exploring micromixing in chemical process.

3.3.3. LMS in promoting reaction selectivity

Apart from increasing the reaction rate, LM microreactor could also enhance the selectivity of reactions. Several experiments were performed to demonstrate this, including reactions (2) and (3) above. Since the molar ratio of $S_2O_8^{2-}$ and I^- was maintained at 1:2, there should be no I^{3-} present under ideal condition. Fig. 9b shows monitoring results in bulk reaction and LM reaction (40 μL; vertical height: 5 cm). It is notable that the I^{3-} concentration in LMs was much lower, meaning the LM microreactor could reach ideal mixing with fewer by-products.

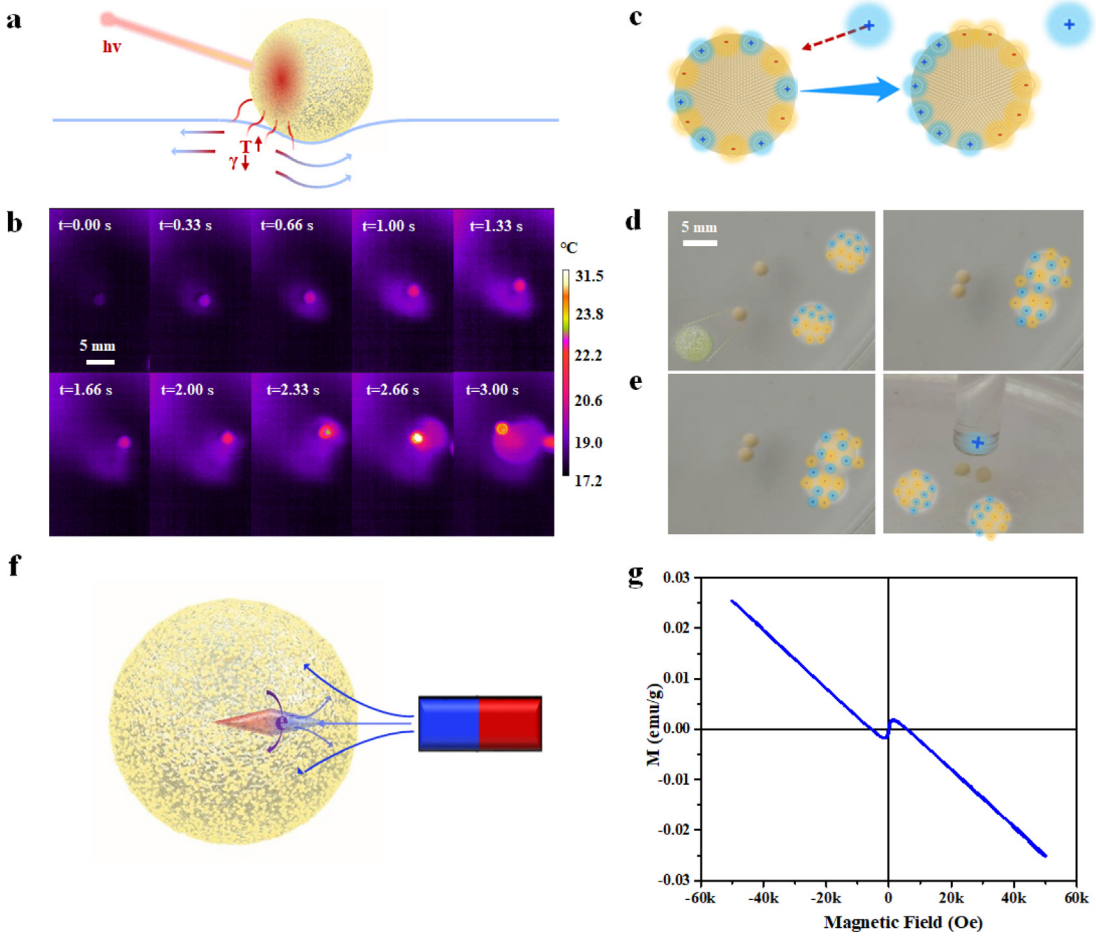

Fig. 5. (a) Scheme illustrating the light-driving locomotion of LMs on the air–water interface. (b) Snapshots of light-driving LMs recorded by thermography. (c) Scheme illustration of voltage-driving movement of LMs. (d) Assembled LMs spontaneously triggered by static electricity. (e) The repulsion between two LMs triggered by a charged glass bar. (f) Schematic diagram of diamagnetism-responsive LMs. (g) Room temperature magnetization loops of CDs@POSS powders.

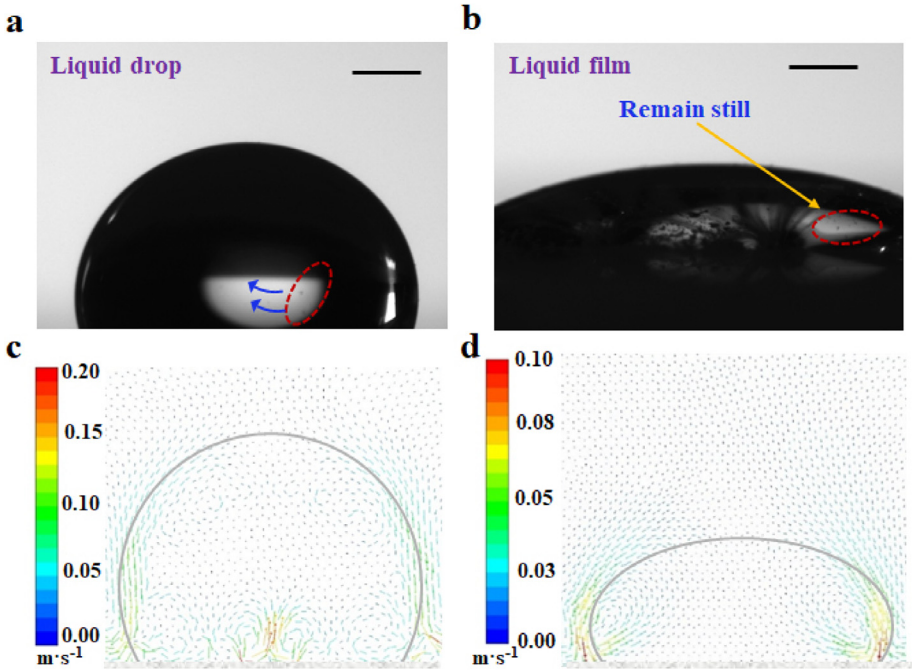

Fig. 6. (a) liquid drop on CDs@POSS powders. (b) liquid film on CDs@POSS powders. All scale bars are 1 mm. Corresponding CFD simulation for (c) liquid drop and (d) liquid film.

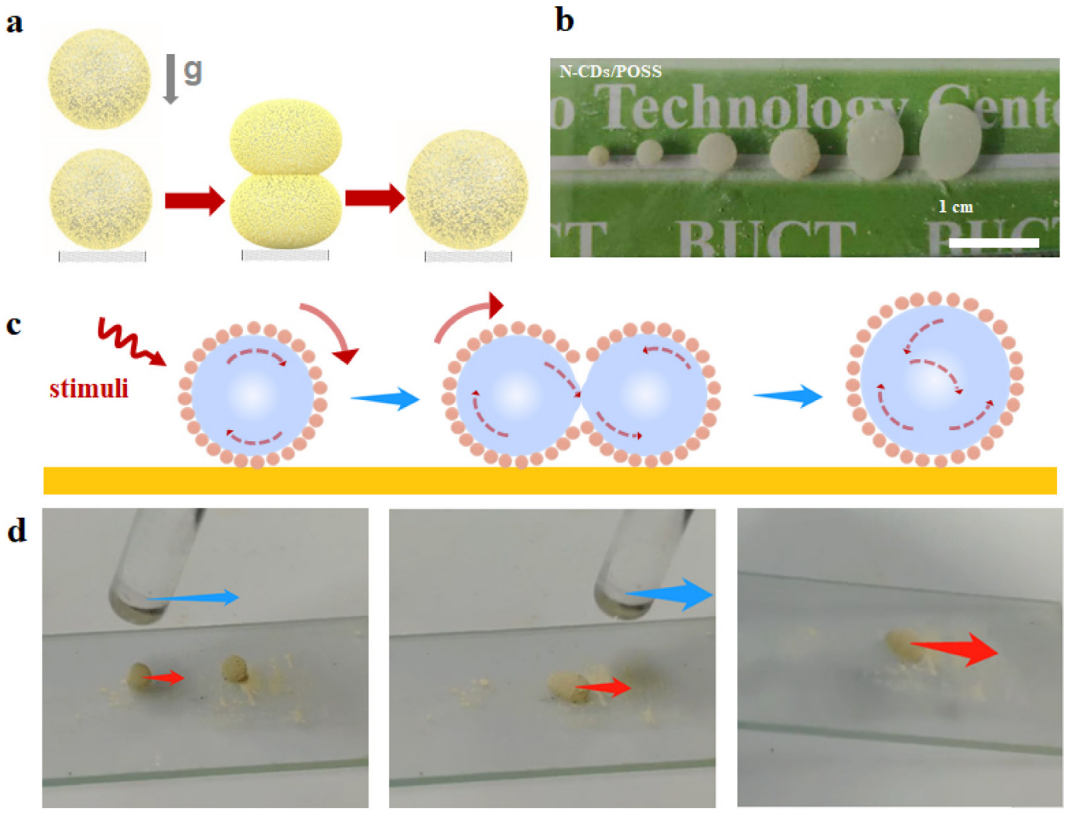

Fig. 7. (a) Schematic illustration of two liquid marbles collided by gravity. (b) Optical photographs of different size LMs. (c) Schematic illustration of colliding-triggered intensification in microreactor by remote stimuli. (d) Collision between LMs triggered by electricity and rolling transfer of the collided LMs.

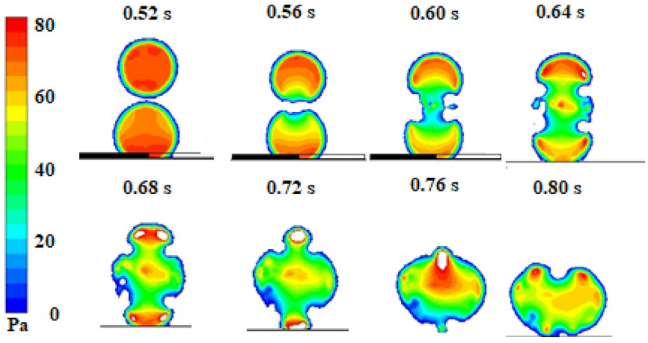

Fig. 8. CFD simulation of collisions between two liquid drops triggered by gravity, along with time.

Another common parallel reaction was also employed to demonstrate this enhancement in reaction selectivity:

$$Na_2CO_3 + HCl = NaHCO_3 + NaCl \quad (4)$$

$$NaHCO_3 + HCl = NaCl + CO_2 + H_2O \quad (5)$$

In this reaction, a molar ratio of Na_2CO_3 and HCl of 1:1 was adopted. TGA analysis was characterized to analyze the composition of products (Fig. 9c). It was revealed that reactions in the LMs exhibited higher mass loss, meaning higher yield of $NaHCO_3$. Additionally, as the LMs became smaller, the reaction selectivity increased. In these experiments, the yield in LMs could reach nearly 100%, whereas the yield in bulk solution remained only 63%. Notably, the optimal size for chemical reactions in our work was 10 μL LMs which could be simply adjusted by changing the volume of liquid droplet. It is foreseeable that smaller LM will extend its potential which remains to be explored, and LMs can be particularlly useful in some hydrocracking processes where reaction selectcity is crucial [41].

3.3.4. LMS as photocatalytic microreactors

Typically, as an attractive fluorescent nanomaterial, CDs can absorb ultraviolet light to emit visible light [36]. Therefore, CDs@POSS-capsulated LMs were believed to act as microreactors with light-induced potential. It avoided complicated and tedious procedures such as constructing a transparent microchannel [37]. To verify the potential application of a photocatalytic microreactor, the photodegradation of methylene blue by the Fenton reaction was performed. Initially, 20 μL LMs containing 5 mM MB solution and 13 mM $FeCl_3$ were prepared, after which H_2O_2 (30% wt, 20 mL) was added. After 10 s, the mixture was analyzed in a 50-fold diluted solution. Fig. 9d indicates that within 15 min reaction time under ultraviolet light (365 nm), 95% of the initial MB was degraded. Compared with the LM reactor without light irradiation, the rate was increased by a factor of 2.6 (Fig. 9e). The inset digital image in Fig. 9d depicts the blue color emission under ultraviolet light, demonstrating the capabilities of LMs with CDs@POSS layer to work as photocatalytic microreactors.

4. Conclusion

In this study, the method of synthesizing CDs@POSS nanoparticles as encapsulating powders for the preparation of multi-stimuli-responsive LMs was developed and demonstrated by characteristic analysis. CDs equip LMs with properties of fluorescence, diamagnetism and photothermic while POSS make them hydrophobic.

Performance and mechanism of external stimuli to trigger LM's movement were studied in this work. Light drove LMs at a maximum rate of 12 $mm{\cdot}s^{-1}$ and its direction could be manipulated sensitively. Surface tension induced Marangoni flow caused by temperature difference between LMs and water was believed to be the source of propulsion. Electricity could drive LMs to reach velocity as high as 6.4 $cm{\cdot}s^{-1}$, which was explained by the electrostatic force (F_E) caused by free-charge migration. Magnetism actuated LMs to move in different

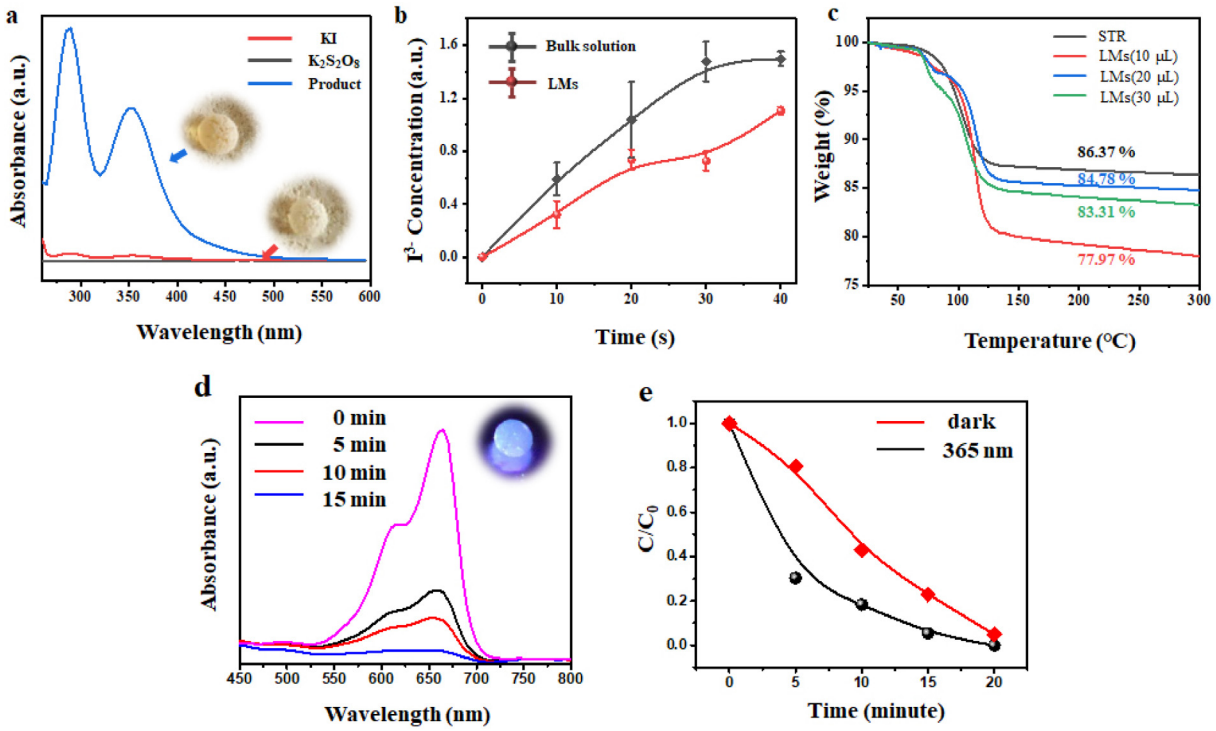

Fig. 9. (a) UV–vis absorption spectra of reactants and products of stimuli-triggered collision micro-reaction. (b) Plots of time-depended I^{3-} concentrations reacted in bulk solution and LMs. (c) TGA of products from reacting sodium carbonate ($NaCO_3$) and hydrochloric acid (HCl) in LMs and STR. (d) UV–vis spectra of methylene blue solutions measured at different times, inset: photoluminescence of CDs@POSS coated LMs. (e) Plots of normalized methylene blue concentrations (C/C_0) operated in darkness (red plot) and under 365 nm laser irradiation (dark plot). (For interpretation of the references to color in this figure legend, the reader is referred to the web version of this article.)

directions as lowly as 2 mm·s^{-1}. Moreover, electricity and magnetism both played a role in reducing friction of LM's locomotion. This shows that various external stimulus exercised different response levels on the locomotion of LMs, so the combined multi-stimuli was expected to provide a more precise control of microfluid.

Furthermore, using external stimuli to bring about collisions between LMs containing different reactants was explored, the resultant CDs@POSS-based LMs can act as ideal miniature reactors triggered by multiple stimuli to enhance reactions. The effect of drop size and collision on reaction rate, reaction selectivity and the size of nanomaterials are systematically studied. Through experiments and simulation of gravity-triggered collision between two LMs, it is found that higher kinetic energy and smaller LMs sizes achieved greater yields with nanoparticle size reduced. Results also show that the LM microreactor provided a promising way of enhancing mixing thus reaction rate and improving reaction selectivity. Notably, LMs could also work as photocatalytic microreactors, which was testified through experiments.

In summary, the CDs@POSS-based LMs have great potential in several applications and could be particularly attractive microreactors due to their abilities of intensifying and selecting reaction process under various external stimuli.

Acknowledgments

We are grateful for financial support from National Natural Science Foundation of China (21620102007, and 21622601), the Fundamental Research Funds for the Central Universities of China (BUCTRC201601), and the "111" project of China (B14004).

Appendix A. Supplementary data

Supplementary data to this article can be found online at https://doi.org/10.1016/j.cej.2019.123478.

References

[1] P. Aussillous, D. Quéré, Liquid marbles, Nature 411 (2001) 924–927.
[2] Z. Liu, Y. Zhang, C. Chen, T. Yang, J. Wang, L. Guo, P. Liu, T. Kong, Larger stabilizing particles make stronger liquid marble, Small 1804549 (2018).
[3] D. Boglaienko, B. Tansel, Submergence patterns of floating crude oil by granular particles, Chem. Eng. J. 314 (2017) 548–553.
[4] C. Fullarton, T.C. Draper, N. Phillips, R. Mayne, B. Costello, A. Adamatzky, Evaporation, lifetime, and robustness studies of liquid marbles for collision-based computing, Langmuir 34 (2018) 2573–2580.
[5] H. Kawashima, M. Paven, H. Mayama, H.-J. Butt, Y. Nakamura, S. Fujii, Transfer of materials from water to solid surfaces by using liquid marbles, ACS Appl. Mater. Inter. 9 (2017) 33351–33359.
[6] J. Vialetto, M. Hayakawa, N. Kavokine, M. Takinoue, S.N. Varanakkottu, S. Rudiuk, M. Anyfantakis, M. Morel, D. Baigl, Magnetic actuation of drops and liquid marbles using a deformable paramagnetic liquid substrate, Angew. Chem. 129 (2017) 16792–16797.
[7] Y. Sun, X. Huang, S. Soh, Solid-to-liquid charge transfer for generating droplets with tunable charge, Angew. Chem. Int. Ed. 128 (2016) 10110–10114.
[8] M. Paven, H. Mayama, T. Sekido, H.-J. Butt, Y. Nakamura, S. Fujii, Light-driven delivery and release of materials using liquid marbles, Adv. Funct. Mater. 26 (2016) 3199–3206.
[9] Z. Chen, D. Zang, L. Zhao, M. Qu, X. Li, X. Li, L. Li, X. Geng, Liquid marble coalescence and triggered microreaction driven by acoustic levitation, Langmuir 33 (2017) 6232–6239.
[10] D. Wang, L. Zhu, J.-F. Chen, L. Dai, Liquid marbles based on magnetic upconversion nanoparticles as magnetically and optically responsive miniature reactors for photocatalysis and photodynamic therapy, Angew. Chem. 128 (2016) 10953–10957.
[11] T.H. Nguyen, K. Hapgood, W. Shen, Observation of the liquid marble morphology using confocal microscopy, Chem. Eng. J. 162 (2010) 396–405.
[12] S. Fujii, S. Yusa, Y. Nakamura, Stimuli-responsive liquid marbles: controlling structure, shape, stability, and motion, Adv. Funct. Mater. 26 (2016) 7198-7198.
[13] W. Ye, X. Li, H. Zhu, X. Wang, S. Wang, H. Wang, R. Sun, Green fabrication of cellulose/graphene composite in ionic liquid and its electrochemical and photothermal properties, Chem. Eng. J. 299 (2016) 45–55.
[14] L. Zhang, D. Cha, P. Wang, Remotely controllable liquid marbles, Adv. Mater. 24 (2012) 756–4760.
[15] Y. Chu, Z. Wang, Q. Pan, Constructing robust liquid marbles for miniaturized synthesis of graphene/Ag nanocomposite, ACS Appl. Mater. Inter. 6 (2014) 8378–8386.
[16] Q. Shang, L. Hu, Y. Hu, Y. Hu, C. Liu, Y. Zhou, Fabrication of superhydrophobic

fluorinated silica nanoparticles for multifunctional liquid marbles, Appl. Phys. A 124 (2018) 25.
[17] L. Shang, Y. Cheng, Y. Zhao, Emerging droplet microfluidics, Chem. Rev. 117 (2017) 7964.
[18] E. Bormashenko, Liquid marbles, elastic nonstick droplets: from minireactors to self-propulsion, Langmuir 33 (2016) 663–669.
[19] Y.E. Miao, H.K. Lee, W.S. Chew, I.Y. Phang, T. Liu, X.Y. Ling, Catalytic liquid marbles: Ag nanowire-based miniature reactors for highly efficient degradation of methylene blue, Chem. Commun. 50 (2014) 5923–5926.
[20] Y. Sheng, G. Sun, J. Wu, G. Ma, T. Ngai, Silica-based liquid marbles as microreactors for the silver mirror reaction, Angew. Chem. Int. Ed. 127 (2015) 7118–7123.
[21] E. Sato, M. Yuri, S. Fujii, T. Nishiyama, Y. Nakamura, H. Horibe, Liquid marbles as a micro-reactor for efficient radical alternating copolymerization of diene monomer and oxygen, Chem. Commun. 51 (2015) 17241–17244.
[22] S. Qin, D. Wang, J.-X. Wang, Y. Pu, J.-F. Chen, Polyhedral oligomeric silsesquioxane-coated nanodiamonds for multifunctional applications, J. Mater. Sci. 53 (2018) 15915–15926.
[23] X. Han, H.K. Lee, Y.H. Lee, Y.H. Lee, X.Y. Ling, Dynamic rotating liquid marble for directional and enhanced mass transportation in three-dimensional microliter droplets, J. Phys. Chem. Lett. 8 (2017) 243–249.
[24] W. Gao, H.K. Lee, J. Hobley, T. Liu, I.Y. Phang, X.Y. Ling, Graphene liquid marbles as photothermal miniature reactors for reaction kinetics modulation, Angew. Chem. 127 (2015) 4065–4068.
[25] X. He, Z. Wang, Y. Pu, D. Wang, R. Tang, S. Cui, J.-X. Wang, J.-F. Chen, High-gravity-assisted scalable synthesis of zirconia nanodispersion for light emitting diodes encapsulation with enhanced light extraction efficiency, Chem. Eng. Sci. 195 (2019) 1–10.
[26] T.C. Draper, C. Fullarton, N. Phillips, B. Costello, A. Adamatzky, Liquid marble interaction gate for collision-based computing, Mater. Today 20 (2017) 561–568.
[27] J. Jin, C.H. Ooi, D.V. Dao, N.-T. Nguyen, Liquid marble coalescence via vertical collision, Soft Matter 14 (2018) 4160–4168.
[28] M.K. Khaw, C.H. Ooi, F. Mohd-Yasin, R. Vadivelu, J.S. John, N.-T. Nguyen, Digital microfluidics with a magnetically actuated floating liquid marble, Lab Chip 16 (2016) 2211–2218.
[29] Z. Liu, X. Fu, B.P. Binks, H.C. Shum, Coalescence of electrically charged liquid marbles, Soft Matter. 13 (2017) 119–124.
[30] D. Wang, Z. Wang, Q. Zhan, Y. Pu, J.-X. Wang, N.R. Foster, L. Dai, Facile and scalable preparation of fluorescent carbon dots for multifunctional applications, Engineering 3 (2017) 402–408.
[31] S. Hu, Y. Wang, W. Zhang, Q. Chang, J. Yang, Multicolour emission states from charge transfer between carbon dots and surface molecules, Materials 10 (2017) 165.
[32] B. Geng, D. Yang, D. Pan, L. Wang, F. Zheng, W. Shen, C. Zhang, X. Li, NIR-responsive carbon dots for efficient photothermal cancer therapy at low power densities, Carbon 134 (2018) 153–162.
[33] Y. Xue, H. Wang, Y. Zhao, L. Dai, L. Feng, X. Wang, T. Lin, Magnetic liquid marbles: A “Precise” miniature reactor, Adv. Mater. 22 (2010) 4814–4818.
[34] T.L. Makarova, Magnetic properties of carbon structures, Semiconductors 38 (2004) 615–638.
[35] X. Luo, H. Yin, X. Li, X. Su, Y. Feng, CO_2-triggered Microreactions in Liquid Marbles, Chem. Commun. 54 (2018) 9119.
[36] Z. Yang, J. Wei, Y.I. Sobolev, B.A. Grzybowski, Systems of mechanized and reactive droplets powered by multi-responsive surfactants, Nature 553 (2018) 313–318.
[37] A. Castedo, E. Mendoza, I. Angurell, J. Llorca, Silicone microreactors for the photocatalytic generation of hydrogen, Catal. Today 273 (2016) 106–111.
[38] N. Kavokine, M. Anyfantakis, M. Morel, S. Rudiuk, T. Bickel, D. Baigl, Light-driven transport of a liquid marble with and against surface flows, Angew. Chem. Int. Edit. 55 (2016) 11183–11187.
[39] C.H. Ooi, A.V. Nguyen, G.M. Evans, D.V. Dao, N.T. Nguyen, Measuring the coefficient of friction of a small floating liquid marble, Sci. Rep. 6 (2016) 38346.
[40] K.R. Sreejith, L. Gorgannezhad, J. Jin, C.H. Ooi, H. Stratton, D.V. Dao, N.T. Nguyen, Liquid marbles as biochemical reactors for the polymerase chain reaction, Lab Chip (2019).
[41] C. Peng, B. Liu, X. Feng, Y. Du, X. Fang, Engineering dual bed hydrocracking catalyst towards enhanced high-octane gasoline generation from light cycle oil, Chem. Eng. J. (2019), https://doi.org/10.1016/j.cej.2019.123461 (in press).